



ELSEVIER

Combustion and Flame 132 (2003) 545–555

**Combustion
and Flame**

Uncertainty quantification in reacting-flow simulations through non-intrusive spectral projection

Matthew T. Reagan^{*,a}, Habib N. Najm^a, Roger G. Ghanem^b,
Omar M. Knio^b

^aSandia National Laboratories, Livermore, CA 94551, USA

^bThe Johns Hopkins University, Baltimore, MD 21286-2686, USA

Received 10 May 2002; received in revised form 20 September 2002; accepted 30 September 2002

Abstract

A spectral formalism has been developed for the “non-intrusive” analysis of parametric uncertainty in reacting-flow systems. In comparison to conventional Monte Carlo analysis, this method quantifies the extent, dependence, and propagation of uncertainty through the model system and allows the correlation of uncertainties in specific parameters to the resulting uncertainty in detailed flame structure. For the homogeneous ignition chemistry of a hydrogen oxidation mechanism in supercritical water, spectral projection enhances existing Monte Carlo methods, adding detailed sensitivity information to uncertainty analysis and relating uncertainty propagation to reaction chemistry. For 1-D premixed flame calculations, the method quantifies the effect of each uncertain parameter on total uncertainty and flame structure, and localizes the effects of specific parameters within the flame itself. In both 0-D and 1-D examples, it is clear that known empirical uncertainties in model parameters may result in large uncertainties in the final output. This has important consequences for the development and evaluation of combustion models. This spectral formalism may be extended to multidimensional systems and can be used to develop more efficient “intrusive” reformulations of the governing equations to build uncertainty analysis directly into reacting flow simulations. © 2003 The Combustion Institute. All rights reserved.

Keywords: Uncertainty, Flame, Simulation, Spectral, Polynomial, Chaos

1. Introduction

Uncertainty quantification (UQ) in computational predictions is useful from an engineering point of view, where confidence intervals on predicted system behavior are necessary for design and optimization of engineering systems. It is also useful from a scientific point of view, where model validation with respect to experimental measurements requires careful mea-

asures of uncertainty in both experimental data and computational predictions. In general, uncertainty in computational results can be due to both model and parametric uncertainty. The present work deals with the latter, which is the easier of these two problems. Specifically, we investigate the propagation of uncertainty from the model parameters to simulation outputs in the context of low Mach number reacting flow modeling, with a focus on supercritical water oxidation (SCWO).

Supercritical water oxidation has been identified as a novel means of treating a wide array of dilute aqueous wastes [1]. At the typical operating conditions of 450 to 600°C and 250 to 280 bar, free-radical oxidation reactions proceed rapidly and completely.

* Corresponding author. Tel.: +1-925-294-2866; fax: +1-925-294-2595.

E-mail address: mtreaga@ca.sandia.gov (M.T. Reagan).

The design of the SCWO process requires the development of appropriate combustion chemistry models. Sources of parametric uncertainty in these models include experimentally-determined reaction rate constants, thermodynamic properties, and transport properties.

In general, the propagation of parametric uncertainty can be studied using Monte Carlo (MC) simulations, with appropriate choices of model parameters over their ranges of uncertainty. However, this approach does not readily provide information about the sensitivity of model outputs to specific parametric uncertainties. An alternative approach is discussed here, based on a spectral stochastic description of uncertain parameters and field quantities. This spectral description makes use of polynomial chaos (PC) expansions [2–8]. Given MC sampling of the stochastic parameters, the corresponding solutions of the deterministic system are evaluated and projected onto the PC basis to compute the spectral mode coefficients. These coefficients are then used to construct probability density functions (PDFs) of the solution, to infer sensitivity to various model parameters, and to highlight the dominant sources of uncertainty.

This non-intrusive spectral projection (NISP) approach, which is based on [9], has the advantage of being applicable to legacy codes, which are run with varying parameters to compute the statistics and spectral mode values. It is important to note that, while NISP provides sensitivity information, it actually goes well beyond sensitivity analysis in that it propagates the full probabilistic representation of the model inputs to the model outputs. Moreover, the NISP-evaluated dependencies are related to the specific uncertainty in a given parameter, while sensitivity analysis compares equal parametric perturbations. Further, depending on the chosen order of the PC expansion, NISP also provides higher-order sensitivity information. Higher-order effects are not lumped into a single coefficient, but are considered independently and in terms of parameter-parameter interactions. The result is a complete PC representation of a complex system response behavior that can be used to generate PDFs of model output in terms of the selected PDFs of model inputs.

Other UQ methods are available, and for certain problems may have efficiency advantages. The deterministic equivalent modeling method (DEMM) [10] is a probabilistic collocation method that generates a PC expansion of model outputs for systems with well-behaved response functions. It limits sampling to a subset of the roots of the next-higher order polynomial chaos. The stochastic response surface method (SRS) [11] expands sampling by using regression to generate coefficients from a complete

set of higher-order roots. Both of these methods give good agreement with Monte Carlo for the estimation of output PDFs, and also fit the probabilistic response function to a set of PC coefficients. However, it is not clear that limiting sampling to the partial or full set of polynomial roots can adequately sample the necessary range of stochastic space, particularly for systems with strongly non-Gaussian responses.

A final comparison should be made with the “intrusive” spectral/pseudospectral methodologies. If it is possible to reformulate the governing equations for a particular problem, numerical efficiency can be gained by creating a purpose-built spectral/pseudospectral code. Each quantity can be represented by a PC expansion, as discussed above. These expansions are substituted into the set of governing equations using a Galerkin approach that takes advantage of the orthogonality of the Hermite polynomials. The result is a system of equations that can be solved simultaneously to provide both mean values and stochastic information [12,13]. Such a reformulation may not be practical with existing complex codes, and therefore a non-intrusive approach may be the most practical way to approach the problem. In this study, we apply the NISP approach to an existing software package, PREMIX [15,16], to demonstrate the utility of a non-intrusive analysis.

In the present work we apply the NISP procedure to two model problems. The first is a homogeneous ignition, a problem where uncertainty propagation has been studied previously by Phenix et al. [10]. The deterministic solver used for modeling ignition uses DVODE [14] for stiff integration of the species equations under constant temperature and pressure conditions. The second is a steady one-dimensional (1-D) premixed hydrogen-oxygen freely-propagating flame at SCWO conditions, computed with the Chemkin PREMIX code. In both instances, we examine the mean and statistics of the solution and evaluate the corresponding spectral PC-modes, given known uncertainties in reaction rate constants and thermodynamic properties of the model based on [10]. We arrive at broad measures of confidence in model predictions, focusing on detailed chemistry. We also identify dominant sources of uncertainty in computed species concentrations, and highlight specific model parameters where reduction of uncertainty via additional experimental measurements can most effectively improve confidence in model predictions.

2. Formulation

The formulation and numerical implementations of the deterministic solvers used for both the ignition and 1-D flame problems are well documented in the

literature [14–16]. We will focus instead on the description of the NISP model.

As mentioned above, we focus on parametric uncertainty. We represent each uncertain model parameter as a stochastic quantity with known probability density function (PDF). Let an uncertain parameter λ be empirically given by

$$\lambda = \bar{\lambda} \pm \hat{\lambda}. \tag{1}$$

where $\bar{\lambda}$ is the mean and $\hat{\lambda}$ defines the range of uncertainty.

Then, with no additional information, we assume that λ is sampled from a Gaussian PDF with a mean λ_0 and a standard deviation λ_1 consistent with Eq. (1). Further, if we let ξ be a normalized Gaussian random variable with zero mean and unit variance we can express λ as

$$\lambda = \lambda_0 + \xi\lambda_1 \tag{2}$$

If, on the other hand, additional physical constraints are in effect, e.g. when λ is a pre-exponential Arrhenius rate constant that is strictly positive, then a lognormal PDF is more suitable. In this case, as discussed in [17,18], λ can be expanded in powers of ξ , with the necessary order dictated by the skewness of the distribution.

For a general prescribed PDF of λ , we can represent λ using the PC expansion

$$\lambda = \sum_{k=0}^P \lambda_k \Psi_k. \tag{3}$$

where the Ψ_k 's are orthogonal Hermite polynomial functions of ξ [8], thus

$$\Psi_k = \begin{cases} 1 & \text{for } k = 0 \\ \xi & \text{for } k = 1 \\ \xi^2 - 1 & \text{for } k = 2 \\ \dots & \end{cases} \tag{4}$$

and the λ_k 's are the known spectral mode strengths of the PC expansion for λ . Note that other functional representations, such as Legendre polynomials, can be used for the Ψ_k 's depending on the nature of the PDFs being considered. In the present context of Gaussian or lognormal PDFs, the Hermite basis is preferred.

More generally, for N uncertain parameters, each parameter introduces a stochastic dimension ξ , such that, with $\theta = \{\xi_1, \xi_2, \dots, \xi_N\}$,

$$\Psi_k = \Psi_k(\theta) = \Psi_k(\xi_1, \xi_2, \dots, \xi_N), \tag{5}$$

$$k = 0, \dots, P.$$

Up to second order, these polynomials are given by:

$$\Psi_k = \begin{cases} 1 & \text{for } k = 0 \\ \xi_k & \text{for } k = 1 \dots N \\ \xi_m \xi_n - \delta_{nm} & \text{for } k = N + 1 \dots P; \\ & m = 1 \dots N; \\ & n = 1 \dots N \end{cases} \tag{6}$$

They are orthogonal with respect to an inner product,

$$\langle \Psi_i \Psi_j \rangle \equiv \int \dots \int \Psi_i(\theta) \Psi_j(\theta) g(\xi_1) \dots g(\xi_N) d\xi_1 \dots d\xi_N \tag{7}$$

where

$$g(\xi) = \frac{e^{-\xi^2/2}}{\sqrt{2\pi}} \tag{8}$$

is a Gaussian measure, and,

$$\langle \Psi_i \rangle = 0, \quad \langle \Psi_i \Psi_j \rangle = 0, \quad i \neq j, \quad i > 0, \quad j > 0 \tag{9}$$

The angle brackets denote the expected value, over the θ space. Using this orthogonality, it is easy to show, starting with the PC expansion for a general parameter λ in Eq. (3) above, multiplying both sides by Ψ_i and taking expectations, that

$$\lambda_i = \frac{\langle \lambda \Psi_i \rangle}{\langle \Psi_i^2 \rangle}, \quad i = 0, \dots, P \tag{10}$$

Further, the model solution u can also be represented using the PC expansion, according to:

$$u(x, t) = \sum_{k=0}^P u_k(x, t) \Psi_k \tag{11}$$

where the u_k 's are the *unknown* spectral modes of u , analogous to the known spectral modes of λ . Again, given the orthogonality of the Ψ_k 's, the u_k 's are given by

$$u_k = \frac{\langle u \Psi_k \rangle}{\langle \Psi_k^2 \rangle}, \quad k = 0, \dots, P \tag{12}$$

The above spectral formulation for parameters and field variables has been used [12] to arrive at reformulated governing equations for the spectral modes u_k . Solving for the spatiotemporal evolution of these modes allows the reconstruction of the evolution of $u(x, t)$ per Eq. (11). On the other hand, this spectral approach requires extensive and specific recoding of an existing numerical code. This can be difficult, and sometimes impractical. An alternative approach focuses on using realizations of the computed deter-

ministic solution to evaluate the expectations in Eq. (12), thereby reconstructing the PC expansion of u . This non-intrusive spectral projection (NISP) procedure is used in the present work.

The NISP procedure involves the following steps:

1. Define PDFs for the model parameters, using known distributions or assuming normal, log-normal, or other general forms.
2. Determine the corresponding spectral PC expansion for each of the parameters.
3. Sample the vector of Gaussians $\theta = \{\xi_1, \xi_2, \dots, \xi_N\}$, and use it to evaluate Ψ_k for $k = 0, \dots, P$ and the corresponding realizations of the vector of parameters $\{\lambda_1, \lambda_2, \dots, \lambda_N\}$, given the determined PC expansions of those parameters.
4. For each realization of the parameters, solve the deterministic problem and compute the corresponding realization of the solution u .
5. Evaluate the above expectations specified in Eq. (12), over a sufficiently large number of samples and find the spectral coefficients u_k of the solution. Thus, for M sample realizations, the modes are found by

$$u_k = \frac{\sum_{m=1}^M (u)_m (\Psi_k)_m}{\sum_{m=1}^M [(\Psi_k)_m]^2}, \quad k = 0, \dots, P \quad (13)$$

where $(\cdot)_m$ denotes the m -th realization.

In this study, the above NISP analysis of simulation results is performed using the DAKOTA toolkit [19,20] using Latin-Hypercube sampling [21] (LHS) for normal random variables. Convergence of the sampling is tracked by examining the maximum standard deviation, calculated directly from the evolving PC expansion. Each LH sample provides a vector of normal random variables ξ_i . These are used to sample from lognormal distributions of the Arrhenius pre-exponential rate constants for the forward reaction rates k_f , and Gaussian distributions of the enthalpies of formation ΔH_f° of the species. The reverse reaction rates are related to the inverse equilibrium constant, which is also log-normally distributed due to its exponential dependence on the Gibbs free energies and therefore the enthalpies of formation [10].

In terms of computational cost, Monte Carlo methods, by design, require many iterations. For the 0-D ignition chemistry, we could perform approximately 125 realizations per hour on a single-processor Pentium III workstation. For 1-D flames, using

the existing Chemkin PREMIX codes, 20 realizations per hour could be expected. For typical runs of 10,000–30,000 samples, this clearly requires considerable computing time. However, the non-intrusive nature of the method described above lends itself to simple parallel distribution of the computing load. Individual machines can process a subset of the samples, using a consistent set of sampling points, and the actual statistics can be compiled through post-processing. The use of multiple independent machines allowed the most intensive calculations to be performed within a reasonable timeframe.

Analysis of the results uses the spectral modes to infer both uncertainty and sensitivity information. To first order in ξ , neglecting second and higher-order terms, we have

$$\frac{\partial u}{\partial \xi_k} = u_k \quad (14)$$

such that the amplitude and sign of a spectral mode is a measure of the influence of the associated parameter on the solution. If identical distributions are assumed for the parameters, this gives a result similar to conventional sensitivity analysis. Note that this sensitivity information ignores the full non-linear coupling of associated species and temperature variations in the system. When comparing flame solutions resulting from different values of the Arrhenius rate constant A_k , the net change in the rate of progress of reaction k is not simply due to the change in A_k , but also due to the associated changes in all species concentrations and temperature. These effects can be quite significant as will be observed below.

3. Results

3.1. 0-D integration of the chemistry

In the previous study by Phenix et al. [10], the DEMM was used with Monte Carlo to propagate uncertainty in supercritical-water oxidation. Using sensitivity analysis, the study developed a reduced variant of the hydrogen oxidation mechanism of Yetter [22] that had proven useful in earlier SCWO modeling studies [23]. This mechanism is given in Table 1. To account for experimental uncertainty, uncertainty in the adaptation of the mechanism to SCWO conditions, and limited stable-species mixture data in supercritical water, each forward rate constant, k_f , was represented by a log-normal probability distribution. The distributions were parameterized via a median value and a multiplicative uncertainty factor, UF , giving upper and lower bounds for each $k_{f,j}$:

Table 1

Reduced hydrogen oxidation mechanism with estimated multiplicative uncertainty factors [10], $k = AT^n \exp(-E_a/RT)$ with units of cm^3 , mol, s, and K.

Reaction			A	n	E_a/R	UF
1. OH + H	\leftrightarrow	H ₂ O	1.620E + 14	0	75	3.16
2. H ₂ + OH	\leftrightarrow	H ₂ O + H	1.024E + 08	1.6	1660	1.26
3. H + O ₂	\leftrightarrow	HO ₂	1.481E + 12	0.6	0	1.58
4. HO ₂ + HO ₂	\leftrightarrow	H ₂ O ₂ + O ₂	1.867E + 12	0	775	1.41
5. H ₂ O ₂ + OH	\leftrightarrow	H ₂ O + HO ₂	7.829E + 12	0	670	1.58
6. H ₂ O ₂ + H	\leftrightarrow	HO ₂ + H ₂	1.686E + 12	0	1890	2.00
7. H ₂ O ₂	\leftrightarrow	OH + OH	3.0000E + 14	0	24400	3.16
8. OH + HO ₂	\leftrightarrow	H ₂ O + O ₂	2.891E + 13	0	-250	3.16

$$\text{Median}(k_{f,j}) \times UF \quad (15)$$

$$\text{Median}(k_{f,j}) \div UF \quad (16)$$

Uncertainty factors used in this analysis and the Phenix study are listed in Table 1. The standard-state enthalpies of formation were modeled as Gaussian distributions, with mean values and standard deviations given in Table 2.

In the DEMM analysis, the response functions were represented as PDFs to estimate the effect of uncertain input parameters. Our NISP analysis also represents the responses in terms of PDFs, but with greatly enhanced sampling of phase space. Since DEMM selects collocation points only from the roots of the next-highest Hermite polynomial, it is not clear that such limited sampling will be effective for all systems, particularly those with larger high-order dependencies. Our analysis also uses the coefficients of the polynomial chaos expansion to characterize the detailed dependencies of each response on each uncertain input parameter.

For this study, we repeated the analysis using NISP techniques and second-order PC expansions. Using the DVODE solver, we integrated the ODE system over a 10s time interval. The vector of random variables ξ_i was used to sample from the reaction rate and enthalpy distributions for 30,000 independent realizations. Each set of sampled parameters was used to integrate the species conservation equa-

tions and to generate profiles of concentration vs. time for each species. The mean and standard deviation for each species concentration was computed, and the concentration profiles were projected onto the PC basis to calculate the deterministic coefficients, $u_k(j, t)$, as functions of species j and time t . The system was integrated at constant $T = 823$ K and $P = 246$ bar, with initial concentrations of $c_{\text{H}_2} = 0.481 \times 10^{-3} \text{ mol/cm}^3$, $c_{\text{O}_2} = 0.243 \times 10^{-3} \text{ mol/cm}^3$, and $c_{\text{H}_2\text{O}} = 0.999 \text{ mol/cm}^3$. While it is also possible to integrate the system with stochastic initial conditions, the present study focuses on uncertainty in reaction rate pre-exponential factors and enthalpies of formation. As such, the statistics and PC mode values evaluated herein necessarily correspond to the above deterministic initial conditions. In the following, spectral mode numbering proceeds from 1 to 8 by reaction number for the pre-exponential rate constants in Table 1, and from 9 to 13 for species H, OH, HO₂, H₂O₂, and H₂O, respectively for the enthalpies of formation in Table 2. Higher-order modes reflect multi-species interaction, as derived from Eq. (6). Species H₂ and O₂ have identically zero enthalpies of formation.

Fig. 1 shows the evolution of OH radical concentration (c_{OH}) vs. time for the reduced chemical system. Upper and lower bounds designate $c_{\text{OH}} \pm \sigma$ as calculated directly from the MC statistics during the NISP production run. This profile outlines the total uncertainty generated by the estimated parametric uncertainty, with 2σ approaching the magnitude of the mean. The results of Phenix et al. [10] showed similar levels of uncertainty for various species, with variations of 70 to 180% from median concentrations. The standard deviation can also be calculated directly from the existing PC coefficients by the summation:

$$\sigma^2 = \sum_{k=1}^P u_k^2 < \Psi_k^2 > \quad (17)$$

Table 2

Mean values and standard deviations of the species standard-state heats of formation ΔH_f° [10].

Species	μ_0	2σ
H	52.10	0.01 kcal/mol
OH	9.3	0.02
H ₂ O	-57.80	0.01
H ₂ O ₂	-32.53	0.07
HO ₂	3.0	0.5

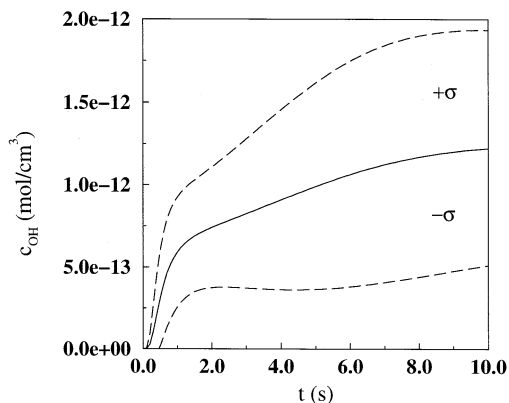


Fig. 1. OH concentration vs. time for 0-D integration of SCWO hydrogen chemistry. The $\pm\sigma$ bounds are calculated directly from the PC expansion.

which produces a similar numerical result for standard deviation as the direct evaluation from the MC statistics. For our system with 13 uncertain parameters (eight reaction pre-exponentials and five enthalpies of formation) and second-order PC expansions, $P = 105$ modes.

The time-evolution of the first-order ($\Psi_k = \xi_k$) spectral modes in the PC-expansion for c_{OH} is shown in Fig. 2. These modes correspond to the propagation of uncertainties in the Arrhenius pre-exponential terms A_k of the forward reaction rates $k_{f,k}$. It is evident that uncertainties in the pre-exponential rate constants of reactions 5, 7, and 8 dominate the expansion and therefore dominate the generation of the total uncertainty in c_{OH} . This is consistent with the

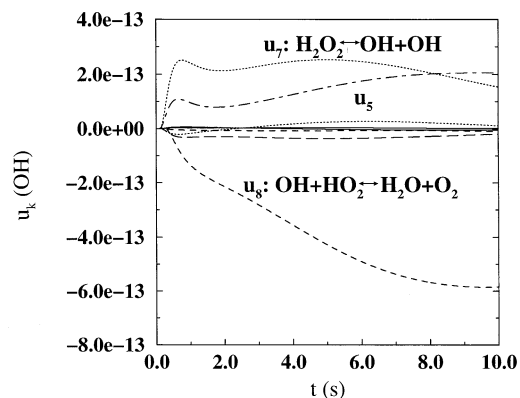


Fig. 2. Spectral decomposition of OH concentration profile for 0-D integration, highlighting the PC coefficients for modes 5, 7, and 8 in units of concentration. These modes represent first-order contribution to the total uncertainty from uncertainty in the corresponding forward reaction rates.

results of Phenix et al. [10], who identified Rn.7 as dominant for the 0-D evolution of the H_2 consumption, although the study did not directly address uncertainty in the concentrations of intermediates. We find Rn.7 to be the dominant OH production channel during the ignition process, while Rn.2 is the dominant OH consumption channel. An increase in A_7 might then be expected to increase OH production and therefore OH concentration, which is indeed observed in Fig. 2 and in the time evolution of c_{OH} . As for Rn.5, its net progress at the unperturbed parameter values is in the reverse direction, thus producing OH, albeit at a relatively small rate. Thus, an increase in A_5 might be expected to lead to an increase in the forward rate of Rn.5, lower OH production and less OH. In fact, we find that increasing A_5 , and the associated changes in species production rates and concentrations, leads to stronger net forward rates of Rns. 2, 3, 4, and 7 in the first 1/2-ms of the ignition process. This leads to a faster OH production rate at early time, and increased overall OH concentration, which is shown by the indicated evolution of u_5 in Fig. 2. Note that the net effect on the rate of progress of Rn.5 is a stronger *reversal*, contributing to the increased rate of OH production. In a similar way, the negative influence of u_8 can be explained based on the overall resultant changes to the reaction network at the larger/smaller A_8 .

It is noteworthy that uncertainties in parameters of Rns. 5 and 8, both somewhat insignificant OH channels, have such a significant impact on the system and lead to large contributions to the total uncertainty in OH prediction. By propagating actual uncertainty values, rather than simply perturbing parameters to gauge sensitivity, we can see how both the influence of a given reaction and the uncertainties associated with reaction rates combine to create a net uncertainty in simulation results. The spectral decomposition not only shows sensitivity information, but also indicates where a given uncertain parameter holds the most influence. In Fig. 2, Rn.7 provides the greatest contribution to uncertainty at $t < 1$ s, with Rn.8 dominating at longer times. Furthermore, the relative dependence of Rns. 5 and 7, and consequently their relative contribution to uncertainty propagation, changes with time as the concentration of OH increases.

Fig. 3 gives mode strengths for u_9 through u_{13} , which represent the first-order variation of $c_{\text{OH}}(t)$ due to uncertainty in the standard-state enthalpies of formation. The importance of $\Delta H_{f,\text{HO}_2}^\circ$ to the total uncertainty is highlighted, in agreement with the observations of Phenix et al. [10]. We also see a significant negative dependence on $\Delta H_{f,\text{OH}}^\circ$, a parameter on which the equilibrium for Rns. 1, 2, 5, 7, and 8 depend.

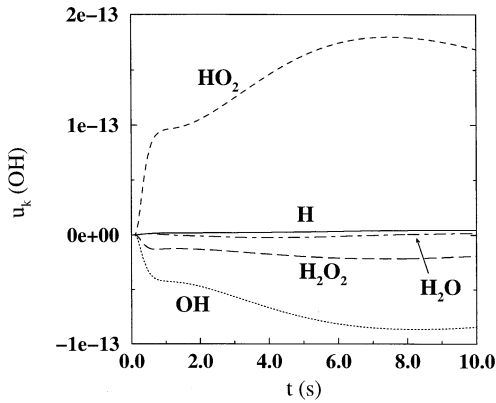


Fig. 3. Spectral decomposition of OH concentration profile for 0-D integration, showing the PC coefficients for first-order modes 9 through 13 in units of concentration. These modes represent the first-order contribution to the total uncertainty from uncertainty in the enthalpies of formation.

In this study, the second-order modes u_{14} to u_{105} , reflecting both higher-order dependence on specific parameters as well as coupling between parameters, are approximately an order of magnitude smaller than first-order mode ($<2.0 \times 10^{-14}$). However, the large number of these modes makes their aggregate contribution to the uncertainty quite significant (up to 50%). Also, for systems with strongly non-Gaussian response behavior, higher-order expansions may become necessary to represent skewed or highly-asymmetrical PDFs. For this particular problem, it is fortuitous that the response functions are well-behaved and can be accurately represented as moderately-skewed Gaussians using second-order PC expansions. This will certainly not be the case for many systems of interest, therefore higher-order analysis and more extensive sampling would be required. NISP allows an arbitrarily high order and large number of samples as computation resources allow.

3.2. 1-D premixed flame simulations

We next extend the NISP technique to the analysis of a 1-D hydrogen flame. We use as our model the Chemkin PREMIX package with SCWO inlet conditions at $T = 823$ K, $P = 246$ bar and a stoichiometric fuel mixture. For this system, the MC integration used 22,000 LH samples from the log-normal and Gaussian distributions for the eight reaction rates and five enthalpies of formation to generate PREMIX input parameters. Convergence was measured by tracking the maximum standard deviation computed directly from the evolving PC expansion. Each flame was normalized to a standard x -coordinate system by matching the point at which the concentration of H_2 has reached 10% of total consumption.

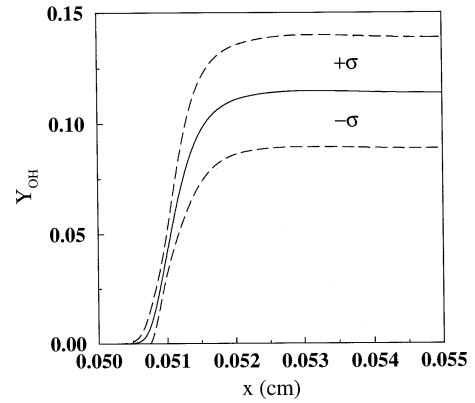


Fig. 4. Profile of OH mass fraction vs. position in the 1-D premixed supercritical-water flame, with $\pm\sigma$ bounds calculated directly from the PC expansion.

In Fig. 4, the mass fraction of OH, $Y_{OH}(x)$, is plotted vs. position. Upper and lower bounds of Y_{OH} , $Y_{OH}(x) \pm \sigma$ are given, calculated directly from the PC expansion. The uncertainty due to the model parameters grows over x , with peak values occurring inside the primary flame reaction zone ($x = 0.0505$ cm to 0.0515 cm). Profiles of the other intermediates and products— HO_2 , H_2O_2 , and H_2O —also show similar localized increases of total uncertainty.

Fig. 5 highlights the four largest first-order modes of Y_{OH} from the spectral decomposition. It is clear that Rn.5 dominates the accumulation of uncertainty within the primary flame. In this case, u_7 is an order-of-magnitude smaller (<0.0002) over all x . The selected modes show how changes in $k_{f,j}$ control the shape of the mass fraction profile of OH. The change

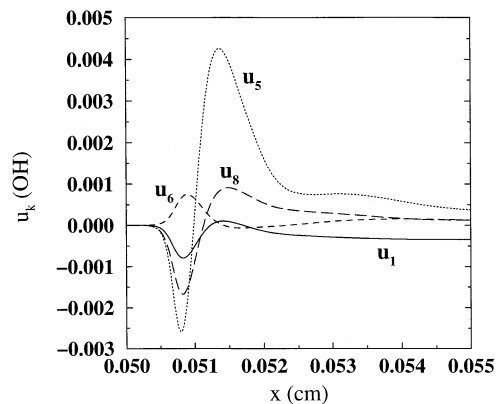


Fig. 5. Spectral decomposition of the OH mass fraction in the 1-D flame, showing the PC coefficients that represent the first-order contribution to the total uncertainty from uncertainty in the forward reaction rates for reactions 1, 5, 6, and 8.

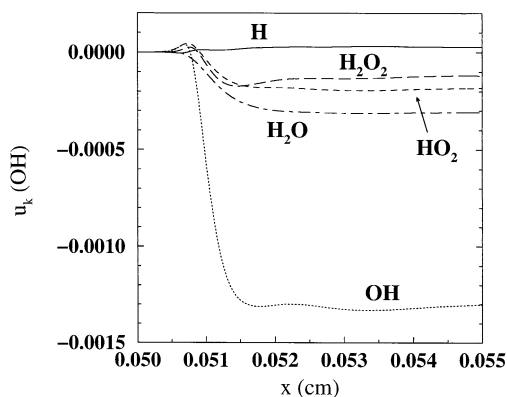


Fig. 6. Spectral decomposition of the OH mass fraction in the 1-D flame, showing the PC coefficients that represent the first-order contribution to the total uncertainty for uncertainty in the enthalpies of formation.

in the sign of u_1 , u_5 , and u_8 near $x = 0.051$ cm corresponds to the inflection point in the $Y_{\text{OH}}(x)$ profile, and highlights the effect of variation in the respective reaction rates on the local slope of the OH profile. Further, the modes describe where, and to what degree, a specific parameter contributes to the total uncertainty in Y_{OH} . Reaction flux analysis (not shown) indicates that Rn.7 dominates OH production in this flame, with a smaller contribution by Rn.5 (net rate in the reverse direction). On the other hand, Rn.2 is the main OH consumer, with lesser contributions by Rns. 1 and 8.

Let us consider the significance of the variation in u_5 in the figure, corresponding to the effect of changes in the pre-exponential Arrhenius term A_5 . Comparison of flame structure between the mean and higher values of A_5 indicates that the slope of the OH profile increases for realizations using larger values of A_5 . The change in the sign of u_5 is a reflection of the difference between the mean OH profile and the higher-slope OH profile. The increase in slope is driven by an increase in the net OH production and consumption rates (not shown), as a result of changes in the rates of *all* the OH reactions towards higher production/consumption. In particular, Rn.5 is found to have a larger net *reverse* rate at the higher A_5 , again reflecting the coupling of changes in all species and temperature associated with the potential variation in A_5 . Here again, we note the significance of a relatively minor production/consumption channel on the overall uncertainty in the predicted species concentration profile despite a comparatively low UF .

Fig. 6 describes the first-order dependence of Y_{OH} on the enthalpies of formation. Here, $\Delta H_{f,\text{OH}}^\circ$ shows the greatest significance, with lesser contributions to the overall uncertainty in OH by the enthalpies of formation of H_2O , HO_2 , and H_2O_2 . As with the 0-D

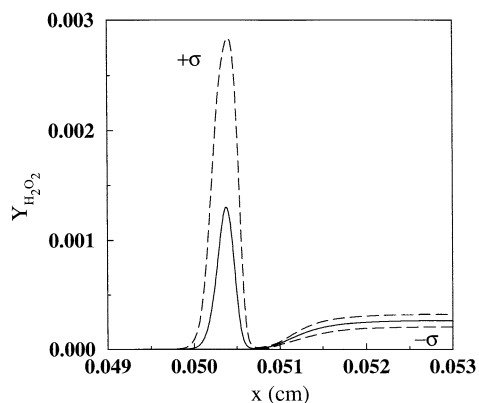


Fig. 7. Profile of H_2O_2 mass fraction vs. position in the 1-D premixed supercritical-water flame, with $\pm\sigma$ bounds calculated directly from the PC expansion.

analysis, the $\Delta H_{f,j}^\circ$ dependencies reflect the roles of the enthalpies of formation in the reaction equilibria, indicating the net sensitivity of the reaction network to particular thermodynamic parameters, the importance of each parameter in uncertainty propagation, and the contribution each enthalpic uncertainty makes to the total uncertainty. All second-order modes were again an order of magnitude smaller, and are not shown.

The analysis is repeated for the H_2O_2 intermediate in Figs. 7–9. For this intermediate, in Fig. 7 we see that the uncertainty in the H_2O_2 mass fraction varies greatly with position, with a maximum uncertainty inside the 1-D flame from $x = 0.0500$ cm to 0.0505 cm, little uncertainty near $x = 0.05075$ cm, and a small, slowly increasing, and eventually constant degree of uncertainty downstream. Tracking the individual realizations of $Y_{\text{H}_2\text{O}_2}$, we find that, for any set of parameters, the mass fraction passes near zero near $x = 0.05075$ cm, resulting in minimum total uncertainty at that point. This uncertainty minimum separates two distinct flame regions, such that the relatively small uncertainty in the post-flame H_2O_2 mass fraction is effectively independent of the larger uncertainty in the primary flame region. Note specifically the *large* uncertainty in H_2O_2 mass fraction within the primary flame, where the standard deviation is larger than the mean. The large range of values of $Y_{\text{H}_2\text{O}_2}$ spanned by the data suggests that the reduced chemical model may lack robustness for predicting this species, given existing uncertainties in chemical and thermodynamic parameters. Reducing the parametric uncertainty in the reaction rates, particularly Rn.5, would reduce the total accumulation of uncertainty in $Y_{\text{H}_2\text{O}_2}$ and enhance the robustness of the model.

In order to identify the causes behind this ob-

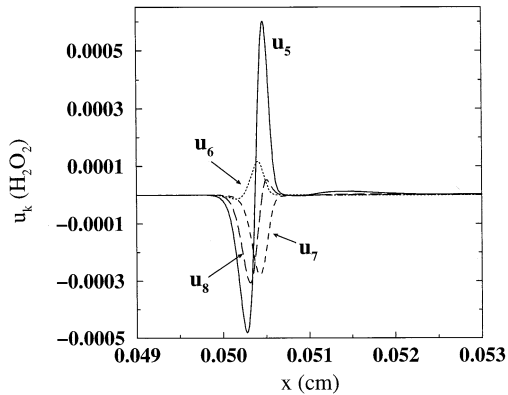


Fig. 8. Spectral decomposition of the H_2O_2 mass fraction in the 1-D flame, highlighting the PC coefficients that represent the first-order contribution to the total uncertainty from uncertainty in the forward reaction rates for reactions 5, 6, 7, and 8.

served uncertainty in $Y_{\text{H}_2\text{O}_2}$, we plot the associated first-order spectral modes in Fig. 8. Here, u_5 again dominates, reaching twice the magnitude of u_7 or u_8 . The decay of all spectral modes to near zero in the vicinity of $x = 0.05075$ cm reflects the above observed minimum in uncertainty at this location. Note that the main production and consumption zones of H_2O_2 in the deterministic/unperturbed flame are to the left of the minimum at $x = 0.05075$ cm, with Rns. 4 and 5 being the dominant production channels, and Rn.7 the dominant consumption channel. The effect of A_5 -uncertainty can again be studied by comparing the flame structure at the mean and high A_5 values. Increasing A_5 leads to an increase in both production and consumption peaks of H_2O_2 (not shown). These are driven by changes in all reaction rates of progress resulting from the change in A_5 and associated change in species concentration and temperature. Particularly significant increases in the production rate of H_2O_2 at $x < 0.05075$ are due to Rns. 4 and 5 (Rn.5 again going in a net reverse direction). A significant increase in consumption of H_2O_2 in this region is due to an increase in the net reverse rate of Rn.7. All of these changes are driven by the increase in A_5 and the associated changes in flame structure. The net result is an increased peak value and smaller width of the $Y_{\text{H}_2\text{O}_2}$ profile—hence larger slopes that, as with OH, create the associated signature observed in the u_5 profile in Fig. 8. Note that u_5 is also the significant source of H_2O_2 uncertainty downstream, as seen in Fig. 8.

The first-order enthalpy-of-formation spectral modes of $Y_{\text{H}_2\text{O}_2}$ are shown in Fig. 9. Uncertainty in the enthalpy of formation of OH is again significant, as well as that of HO_2 . On the other hand, these amplitudes are small compared to those resulting

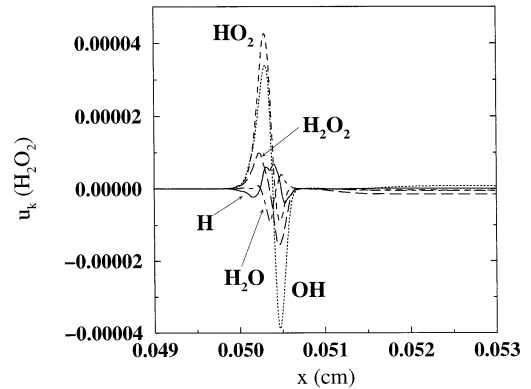


Fig. 9. Spectral decomposition of the H_2O_2 mass fraction in the 1-D flame, highlighting the PC coefficients that represent the first-order contribution to the total uncertainty from uncertainty in the enthalpies of formation.

from the uncertainties in rate constants, in Fig. 8, and therefore have lesser impact on the robustness of the chemical model.

A similar analysis performed for other species reveals that A_5 and $\Delta H_{f,\text{OH}}^o$ are the dominant parameters for all species mass fraction profiles in this mechanism. Clearly, a reduction of the experimental uncertainty in both of these quantities (as well as in $\Delta H_{f,\text{HO}_2}^o$) will have a large impact towards improving robustness of the chemical SCWO model and increasing confidence in model predictions.

One feature that can be discerned through a spectral analysis of uncertainty is not only to what degree, but where and when do particular parametric uncertainties manifest themselves. In Figs. 2 and 3 and in Figs. 5 and 6, we see that a parameter's contribution to total uncertainty can vary with time or flame position and that different parameters propagate uncertainty in different chemical regimes. In Fig. 8 and Fig. 9, it is difficult to discern the relative importance of the modes due to the large changes in mode strength associated with $Y_{\text{H}_2\text{O}_2}$. To better clarify this behavior, Fig. 10 separates the chemical and thermodynamic effects of uncertainty propagation into Y_{OH} in terms of contribution to the standard deviation. Shown are the partial standard deviations computed directly from selected first-order modes of the PC expansion using Eq. 17. The uncertainty contributed through chemical reaction pre-exponential uncertainties can be seen in the shaded curves, with combinations of Rns. 1 and 6, Rns. 1, 6, and 8, and Rns. 1, 6, 8, and 5 highlighted. The dotted line gives the total contribution due to all 1st-order modes, chemical and thermodynamic. It is clear that chemical uncertainties dominate propagation in the flame front, while the remaining thermodynamic parameters become increasingly important in the products side of the flame

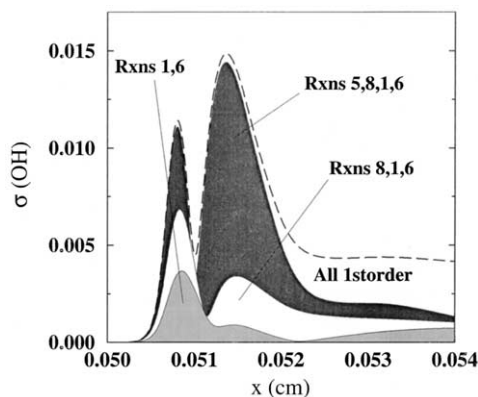


Fig. 10. Standard deviation of OH mass fraction vs. position, comparing the cumulative contribution from first-order dependencies on selected reactions 5, 8, 1, and 6, and the total first-order contribution from all reaction uncertainties and all enthalpic uncertainties.

as the products approach equilibrium downstream of the flame. The enthalpy-propagated uncertainty reaches a constant value, while the chemistry-propagated uncertainty slowly decreases in relative importance several centimeters downstream from the flame.

4. Conclusions

A generalized, non-intrusive spectral projection scheme has been implemented to propagate parametric uncertainty in reacting-flow simulations. Compared to global Monte Carlo estimation of total uncertainty, spectral methods quantify the source of the uncertainty, the propagation of uncertainty through the model, and the sensitivity of model outputs to specific parameters.

For homogeneous ignition chemistry, NISP provides sensitivity information that is consistent with previous work. Quantification of spectral modes adds an additional level of understanding, identifying the significance of individual uncertain parameters and determining where within the evolution of the system each parameter has influence. Extending the analysis to a simple 1-D problem allows the analysis of uncertainty propagation in different regions of a premixed flame, identifying relationships between parameters, specific flame features, and the total propagation of uncertainty.

The consequences of such an analysis are significant. The dramatic amplification of parametric uncertainty within a particular chemical model may call into question the robustness of the model. Further, highlighting the parameters primarily responsible for

the large uncertainty in model outputs is a valuable indicator of where additional experimental measurements may best be targeted. In the particular SCWO system at hand, parameters that merit further measurements are the rate of Rn.5 and the enthalpies of formation of OH and HO₂, as well as the rates of Rns. 7 and 8. Better estimates of these parameters should improve the overall ability of the model to represent the system being studied.

In comparison to the DEMM and SRSM method used before, this method provides similar stochastic information while making fewer assumptions about the system response. For systems with simple, Gaussian-like responses, convergence should be quick and efficient. For more complex systems, particularly chemical systems subject to the positive-concentration constraint, $c_i \geq 0.0$, higher-order terms are likely to be significant for intermediates or during the early stages of an ignition problem. Unphysical PDFs (distributions with significant probabilities for negative concentrations) or non-convergent expansions (PC coefficients increasing with increasing order) would indicate that the selected order is not sufficient to represent the system response.

This analysis is readily extendable to multiple dimensions and greater numbers of uncertain parameters, while preserving the integrity of the realization engine through the non-intrusive operation of the method. Further, using the above spectral stochastic formulation, a Galerkin approach can be used to derive governing equations for the spectral mode coefficients directly. This intrusive approach obviates the need for MC computations at the cost of a reformulation of the governing equations. It offers the potential advantage of computational savings, as the resulting system can be easier to compute than a large number of MC simulations. However, the reformulation of the problem may not be practical for legacy codes, proprietary codes, one-time analyses, or large-scale codes that are not required to apply uncertainty analysis to each application. While outside the scope of this paper, application of intrusive methods to non-reacting flow can be found in [12,13], and an extension to general chemical kinetics is in progress.

Acknowledgments

This work was supported through the Laboratory Directed Research and Development program at Sandia National Laboratories funded by the U.S. Department of Energy, and by the DOE Office of Basic Energy Sciences (BES), Division of Chemical Sciences, Geosciences and Biosciences.

References

- [1] J. Tester, H. Holgate, F. Armellini, P. Webley, W. Killilea, G. Hong, H. Barner, Emerging technologies for hazardous waste management, American Chemical Society, 1993.
- [2] N. Wiener, *Amer. J. Math.* 60 (1938) 897–936.
- [3] R. Cameron, W. Martin, *Ann. Math.* 48 (1947) 385–392.
- [4] A. Chorin, *J. Comp. Phys.* 8 (1971) 472–482.
- [5] F. Maltz, D. Hitzl, *J. Comp. Phys.* 32 (1979) 345–376.
- [6] W. Meecham, D. Jeng, *J. Fluid Mech.* 32 (1968) 225.
- [7] A. Chorin, *J. Fluid Mech.* 63 (1974) 21–32.
- [8] R. Ghanem, P. Spanos, *Stochastic Finite Elements: A Spectral Approach*, Springer Verlag, 1991.
- [9] R. Ghanem, J. Red-Horse, A. Sarkar, 8th ASCE Specialty Conference of Probabilistic Mechanics and Structural Reliability, ASCE, 2000.
- [10] B. Phenix, J. Dinero, M. Tatang, J. Tester, J. Howard, G. McRae, *Combust. Flame* 112 (1998) 132–146.
- [11] S. Isukapalli, A. Roy, P. Georgopoulos, *Risk Analysis* 18(3) (1998) 351–363.
- [12] O. Le Maître, O. Knio, H. Najm, R. Ghanem, *J. Comp. Phys.* 173 (2001) 481–511.
- [13] O. Le Maître, M. Reagan, H. Najm, R. Ghanem, O. Knio, *J. Comp. Phys.* 181 (2002) 9–44.
- [14] P. Brown, G. Byrne, A. Hindmarsh, *SIAM J. Sci. Stat. Comput.* 10 (1989) 1038–1051.
- [15] R. Kee, F. Rupley, J. Miller, Sandia Report SAND89–8009B, Sandia National Labs., Livermore, CA, 1993.
- [16] R. Kee, J. Grcar, M. Smooke, J. Miller, Sandia Report SAND85–8240, Sandia National Labs., Livermore, CA, 1993.
- [17] R. Ghanem, *ASME J. Appl. Mech.* 66(4) (1999) 964–973.
- [18] S. Sakamoto, R. Ghanem, *ASCE J. Eng. Mech.* 128(2) (2002) 190–201.
- [19] M. Eldred, Technical report, Sandia Technical Report SAND98–0340, 1998.
- [20] S. Wojtkiewicz, M. Eldred, R. Field, A. Urbina, J. Red-Horse, Proceedings of the 42nd AIAA/ASME/ASCE/AHS/ASC Structures, Structural Dynamics, and Materials Conference, 2001.
- [21] M. McKay, R. Beckman, W. Conover, *Technometrics* 21 (1979) 239–245.
- [22] R. Yetter, F. Dryer, H. Rabitz, *Combust. Sci. Technol.* 79 (1991) 97.
- [23] H. Holgate, J. Tester, *Combust. Sci. Technol.* 88 (1993) 369.